The Astrophysical Journal, 633:1–10, 2005 November 1

EFFECTS OF GRAVITATIONAL EVOLUTION, BIASING, AND REDSHIFT SPACE DISTORTION ON TOPOLOGY

Changbom Park and Juhan Kim
Korea Institute for Advanced Study, 207-43 Cheongryangri-dong, Dongdaemun-gu, Seoul 130-722, South Korea

and

J. Richard Gott III
Department of Astrophysical Sciences, Princeton University, Peyton Hall, Ivy Lane, Princeton, NJ 08544-1001
Received 2005 February 8; accepted 2005 March 25

ABSTRACT

We have studied the dependence of topology of large-scale structure on tracer, gravitational evolution, redshift space distortion, and cosmology. A series of large *N*-body simulations of the ΛCDM and SCDM models that have evolved 1.1 or 8.6 billion particles are used in the study. Evolution of the genus statistic, used as a topology measure, from redshift 8 to 0 is accurately calculated over a wide range of smoothing scales using the simulations. The tracers of large-scale structure considered are the cold dark matter (CDM), biased peaks in the initial density field, dark halos, and "galaxies" populating the dark halos in accordance with a halo occupation distribution (HOD) model. We have found that the effects of biasing, gravitational evolution, and initial conditions on topology of large-scale structure are all comparable. The redshift space distortion effects are relatively small down to about 5 h^{-1} Mpc for all tracers except for the high-threshold part of the genus curve. The gravitational effects are found to be well modeled by analytic perturbation theory when the CDM distribution is considered. But the direction of gravitational evolution of topology can be even reversed for different tracers. For example, the shift parameter of the genus curve evolves in opposite directions for matter and HOD galaxies at large scales. At small scales, there are interesting deviations of the genus curve of dark halos and galaxies from that of matter in our initially Gaussian simulations. The deviations should be understood as due to combined effects of gravitational evolution and biasing. This fact gives us an important opportunity: topology of large-scale structure can be used as a strong constraint on galaxy formation mechanisms. At scales larger than 20 h^{-1} Mpc all the above effects gradually decrease. With good knowledge of the effects of nonlinear gravitational evolution and galaxy biasing on topology, one can also constrain the Gaussian random phase initial conditions hypothesis to high accuracy.

Subject headings: cosmology: theory — large-scale structure of universe — methods: *n*-body simulations

1. INTRODUCTION

Topology analysis has long been applied to galaxy redshift survey data to test one of the major predictions of simple inflationary scenarios: that the primordial density fluctuations are of Gaussian random phase (Gott et al. 1986, 1989; Vogeley et al. 1994). To recover the primordial density fluctuations it is necessary to smooth the observed sample over large enough scales to reach the linear regime. Since redshift surveys have not been very deep in the past, one was left with a small dynamic range for topology study after large smoothings, and it has been hard to draw firm conclusions on the nature of the initial density field. As ambitious new redshift surveys such as the Two Degree Field Galaxy Redshift Survey (2dFGRS) and the Sloan Digital Sky Survey (SDSS)[1] are being completed, it is now hoped that the topology analysis can become one of the precision measures for cosmology. These surveys are not just large in angle and deep in depth, but they are also dense. This means that the new survey samples can be used to study the primordial density field at large scales and also to explore small-scale phenomena like the formation of galaxies.

Since the main purpose of studying topology has been to discover the Gaussianity of the linear density field, there has been relatively little work on topology at small nonlinear scales. One work on small-scale topology is Springel et al. (1998), who applied the analysis to their *N*-body simulations and the 1.2 Jy *Infrared Astronomical Satellite* (*IRAS*) galaxy sample. However, without quantitatively studying the complete scale and cosmology dependences of topology, as measured by the genus, they have incorrectly concluded that the shape of the genus curve is that of a random-phase field far into the nonlinear regime and that the amplitude drop of the genus curve due to the phase correlation is the only sensitive measure of nonlinearity. In this paper we show that topology analysis becomes useful when a sample is studied over a wide range of smoothing scales and when quantitative measures of the deviation of the genus curve from the Gaussian one are used. In particular, we present our finding that topology of underdense regions at small scales is sensitive to the structure formation mechanism. This fact opens the possibility that galaxy formation can be better understood by studying the small-scale topology of galaxy distribution.

Previous analyses of observational samples for topology study have generally used the dark matter distribution for comparison. The similarity of the observed genus curves to those obtained from simulated matter distribution has been investigated for various cosmogonies. This may be fine when the uncertainties in genus measured from observations are much larger than the effects of biasing and redshift space distortion. With the unprecedented accuracy provided by observational data such as the SDSS sample, however, these effects have to be accurately accounted for. In this paper we study the gravitational evolution of the genus of peaks in the initial density field and dark halos as well as

[1] See http://sdss.org.

dark matter to see the dependence of topology on these tracers. Redshift space distortion effects are also studied. They all have nonnegligible, important effects on the genus curve.

Our work is numerical, since our main purpose is to explore the strong nonlinear effects of gravitational evolution through topology analysis, for which current analytic approaches are inadequate. Study of the tracer dependence of, and biasing effects on, topology also requires numerical simulations. To answer the important question of whether the topology is consistent with Gaussian random phase initial conditions to high accuracy in the new large observational data sets, given that the effects of nonlinear evolution and biasing are detectable in such surveys, the best method would seem to be direct comparison with large cosmological simulations with Gaussian random phase initial conditions, where nonlinear evolution and biasing are properly modeled. If agreement is obtained, this supports the Gaussian random phase initial conditions hypothesis to high accuracy.

Introduction to the genus and its related statistics is given in §§ 2 and 3. Our *N*-body simulations used in this study are described in § 4. Evolution of the genus curve is studied in § 5 for matter and "galaxy" distributions in the ΛCDM and SCDM cosmogonies. Conclusions follow in § 6.

2. GENUS

To measure topology of a tracer distribution, we calculate the genus of isodensity surfaces as a function of density threshold level. The genus is defined as

$$G = \text{Number of holes in contour surfaces} - \text{Number of isolated regions} \quad (1)$$

in the isodensity surfaces at a given threshold level. In this definition, a sphere has a genus of -1, and a torus has a genus of 0 (Gott et al. 1986). The Gauss-Bonnet theorem connects the global topology with an integral of local curvature of the surface *S*, i.e.,

$$G = -\frac{1}{4\pi}\int_S \kappa\, dA, \quad (2)$$

where κ is the local Gaussian curvature. The genus is equal to $-\frac{1}{2}$ times the Euler characteristic or the fourth Minkowski functional in three dimensions (Mecke et al. 1994; Schmalzing & Buchert 1997).

For a Gaussian random field, an analytic formula exists for the genus-threshold density relation (Hamilton et al. 1986). The genus per unit volume is

$$g(\nu) = A\left(1-\nu^2\right)e^{-\nu^2/2}, \quad (3)$$

where $\nu \equiv (\rho - \bar{\rho})/\sigma$ is the threshold density in units of standard deviations $\sigma = \langle(\rho-\bar{\rho})^2\rangle^{1/2}$ from the mean. The amplitude is

$$A = \frac{1}{(2\pi)^2}\left(\frac{\langle k^2\rangle}{3}\right)^{3/2}, \quad (4)$$

where the second moment

$$\langle k^2\rangle = \frac{\int P(k)W(k)k^2\, d^3k}{\int P(k)W(k)\, d^3k} \quad (5)$$

depends only on the shape of the power spectrum and the smoothing kernel *W*. Instead of using ν to identify isodensity contours, we use the volume fraction label ν_f at which the corresponding isodensity contours enclose the fraction of the sample volume equal to that at the density threshold $\nu_f\sigma$ in the case of a Gaussian field. In this way the genus curve becomes independent of the one-point probability distribution function, which can be better studied by different statistics. Use of ν_f also makes the genus curves less sensitive to details of bias (Park & Gott 1991), which is beneficial in studying the primordial field.

3. GENUS-RELATED STATISTICS

3.1. *Shift Parameter*

Any departure of the genus curve from the relation given by equation (3) indicates non-Gaussianity of the field. To quantify the deviation we define a set of genus-related statistics. The first statistic $\Delta\nu$ measures the shift of the middle part of the genus curve. We compute $\Delta\nu$, defined by (Park et al. 1992)

$$\Delta\nu = \frac{\int_{-1}^{1}\nu G_{\rm obs}(\nu)\, d\nu}{\int_{-1}^{1} G_{\rm fit}(\nu)\, d\nu}, \quad (6)$$

where $G_{\rm obs}(\nu)$ is the measured genus and $G_{\rm fit}(\nu)$ is the random-phase curve best fitted to the measured genus data from $\nu = -1$ to +1. The best-fitting amplitude $A_{\rm obs}$ of the observed genus curve is obtained from $G_{\rm fit}(0)$.

3.2. *Amplitude Drop*

The second statistic is the amplitude drop of the genus curve. The density field with phase correlation due to gravitational evolution typically has a smaller number of structures compared to that with the same power spectrum (PS) but with random phases. A derived statistic is

$$R_A = \frac{A_{\rm obs}}{A_{\rm PS}}, \quad (7)$$

where $A_{\rm PS}$ is the amplitude expected for a Gaussian field, which has the PS of the evolved particle/galaxy distribution. Existence of phase correlation reduces R_A below 1 (Vogeley et al. 1994; Canavezes et al. 1998). The best-fitting amplitude $A_{\rm obs}$ is measured as explained above. To calculate $A_{\rm PS}$ the PS of the distribution is needed. In this study tracers are contained in simulation cubes with periodic boundaries, and the PS is obtained by Fourier transforming the distribution. Extrapolations of the PS beyond the observed *k*-window necessary to calculate the integral for $A_{\rm PS}$ introduce only a small error in $A_{\rm PS}$ when $\bar{d}/\sqrt{2} \le R_G \le r_{\rm max}/10$, where R_G is the Gaussian smoothing length, $\bar{d}$ is the mean tracer separation, and $r_{\rm max}$ is the sample size.

3.3. *Cluster/Void Abundance Parameters*

The third statistic is the number of clusters and voids. The statistic A_C is defined as

$$A_C = \frac{\int G_{\rm obs}(\nu)\, d\nu}{\int G_{\rm fit}(\nu)\, d\nu}, \quad (8)$$

where the integral is limited to $1.2 \le \nu \le 2.2$, which is roughly centered at $\nu = \sqrt{3}$, which is the minimum in the best-fit random-phase curve where the number of isolated clusters is greatest. Here A_V is similarly defined over $-2.2 \le \nu \le -1.2$ roughly centered at $\nu = -\sqrt{3}$, the minimum in the best-fit random-phase curve where the number of isolated voids is greatest. Here the best-fit Gaussian curve $G_{\rm fit}$ is obtained as explained above using the

TABLE 1
CHARACTERISTICS OF COSMOLOGICAL *N*-BODY SIMULATIONS

Name	Ω_m	Ω_Λ	h	b	N_m[a]	N_p	L (h^{-1} Mpc)	z_i	$N_{\rm step}$	Code
LCDM 1024.....	0.27	0.73	0.71	1.11	2048^3	2048^3	1024	17	680	PM + tree
LCDM 5632.....	0.27	0.73	0.71	1.11	2048^3	2048^3	5632	17	170	PM + tree
LCDM 410.....	0.27	0.73	0.71	1.11	2048^3	1024^3	409.6	47	470	PM
SCDM 1024.....	1.00	0.00	0.5	1.5	2048^3	1024^3	1024	23	230	PM
SCDM 410.....	1.00	0.00	0.5	1.5	2048^3	1024^3	409.6	47	470	PM

[a] Size of mesh on which initial conditions are defined.

middle part of the genus curve. The statistics A_C and A_V quantify the asymmetry of the genus curve and the multiplicity of clusters and voids.

4. SIMULATIONS

In order to study the behavior of the genus statistic accurately, we have made a set of large *N*-body simulations using particle-mesh (PM) and PM + tree codes. Our PM code uses the triangular shaped cloud method for mass assignment and force interpolation at particle positions. The force calculation at mesh points is done by the four-point finite difference algorithm (Park 1990, 1997). The PM + tree code GOTPM, which is a merged version of our PM code with Dubinski's tree code, is a parallel code that adds the tree force to the PM force at separations shorter than 4 times the pixel size of the mesh used in the PM part (Dubinski et al. 2004). For topology study of the matter distribution, the PM code is preferred, since this code can make simulations with large dynamic range in mass at relatively low cost. The PM code is also preferred when the peaks in the initial density field are used as biased tracers because high-resolution initial density fields are adopted in this code. Due to its high force resolution power, the PM + tree code should be the choice when dark halos are targets for topology study. Because a single simulation cannot satisfy all of our needs, we have made several simulations supplementing one another using the PM and PM + tree codes. Parameters of our simulations are summarized in Table 1.

Our results are mainly derived from PM + tree simulations of the ΛCDM model with the *Wilkinson Microwave Anisotropy Probe* (*WMAP*) parameters, namely, the density parameters $\Omega_m = 0.27$ and $\Omega_\Lambda = 0.73$, the Hubble constant $h = 0.71$, $\sigma_{m,8} = 0.9$, and the matter dominated by the cold dark matter (CDM). Here $\sigma_{m,8}$ is the rms mass fluctuation in a sphere of radius of 8 h^{-1} Mpc. The physical sizes of the two simulation cubes are $L = 1024$ and 5632 h^{-1} Mpc. We call them LCDM 1024 and LCDM 5632. We use the transfer function of the power spectrum given by Bardeen et al. (1986) for LCDM 1024, but we use the power spectrum of Eisenstein & Hu (1998) with $\Omega_{\rm baryon} = 0.0463$ for LCDM 5632 to include baryonic effects. The number of CDM particles evolved in both simulations is $2048^3 = 8.59$ billion, among the largest *N*-body simulations ever made. A 2048^3 mesh is used for the PM part, and the force softening length in the tree part is one-tenth of the mean particle separation. Therefore, the dynamic range in length is 2×10^4, from 0.05 to 1024 h^{-1} Mpc, while the dynamic range in mass is 8.6×10^9, from 9.4×10^9 to 8.0×10^{19} $h^{-1} M_\odot$ in the case of LCDM 1024, for example. Dark halos are identified in the LCDM 1024 simulation made by the PM + tree code. Halo centers are found as local density peaks defined on a fine mesh. The CDM particles belonging to virialized dark halos are searched by checking their binding energy to the local halo centers and tidal radii of subhalos with respect to adjacent larger halos (Kim & Park 2005). These identification criteria overcome many of the problems and artificial results obtained from existing group-finding algorithms and allow us to obtain a catalog of self-bound physical dark halos. Only the dark halos with more than 53 member particles or heavier than 5×10^{11} $h^{-1} M_\odot$ are adopted.

Although our group-finding algorithm allows us to identify many subhalos contained in large halos, those halos with mass much higher than 10^{13} $M_\odot$ cannot be considered to be a single galaxy. On the other hand, every halo identified in the *N*-body simulation might not contain a galaxy. Therefore, although dark halos might be better tracers of the observed galaxies than matter, they are still biased tracers. We address this problem by introducing the halo occupation distribution (HOD) prescription to locate "galaxies" within our dark halos. We adopt the following recipe of Zehavi et al. (2005). A central galaxy is assigned to a halo if its mass M exceeds $M_{\rm min}$, and the central galaxy can have satellites. The mean number of satellite galaxies is given by a power law $\langle N_{\rm sat}\rangle = (M/M_1)^\alpha$, and they have a Poisson distribution. We use, as a toy model, the HOD parameters of $\log M_{\rm min} = 11.76$, $\log M_1 = 13.15$, and $\alpha = 1.13$ given by Table 3 of Zehavi et al., corresponding to galaxies with an absolute r magnitude cut of $M_r = -19.5$ in the SDSS. These galaxy tracers are used in § 5.3.

As an another galaxy formation model we adopt the biased galaxy formation scenario in which galaxies form at peaks in the initial density field (Bardeen et al. 1986). We use PM simulations of 1024^3 CDM particles in a 2048^3 mesh spanning 409.6 h^{-1} Mpc along a side. In the ΛCDM model a set of peak bias parameters, $\nu_{\rm th} = 0.05$ and $R_s = 0.763$ h^{-1} Mpc, gives us peak particles that cluster like bright galaxies at the present epoch, where $\nu_{\rm th}$ is the threshold density level for the peaks and R_s is the Gaussian smoothing length corresponding to the galaxy scale. In the case of the SCDM model, the peak parameters adopted are $\nu_{\rm th} = 1.7$ and $R_s = 0.585$ h^{-1} Mpc for $\sigma_{\rm mass,8} = 0.6$. These peak particles have been shown to follow the centers of collapsed dark halos but are too clustered in high-density regions, since no merging process is included (Park & Gott 1991).

5. RESULTS

We have measured the genus statistics in the four-dimensional space of smoothing scale, redshift, tracers, and cosmogony. We use Gaussian smoothing, and the definition of the smoothing length R_G is standard ($\sqrt{2}$ times larger than the "e-folding" smoothing adopted by Gott et al. 1989). We always maintain the condition that the Gaussian smoothing length R_G must be greater than or equal to the mean particle/halo separations. Topology is explored at 14 smoothing scales from $R_G = 1.5$ to 30 h^{-1} Mpc in the case of the matter distribution. Our large and high-resolution simulations enable us to obtain very accurate genus values. The number of resolution elements in the simulation box is over 2500 [$=L^3/(2\pi)^{3/2}R_G^3$] at the largest smoothing scale $R_G = 30$ h^{-1} Mpc and exceeds 2×10^7 at $R_G = 1.5$ h^{-1} Mpc. The genus is also

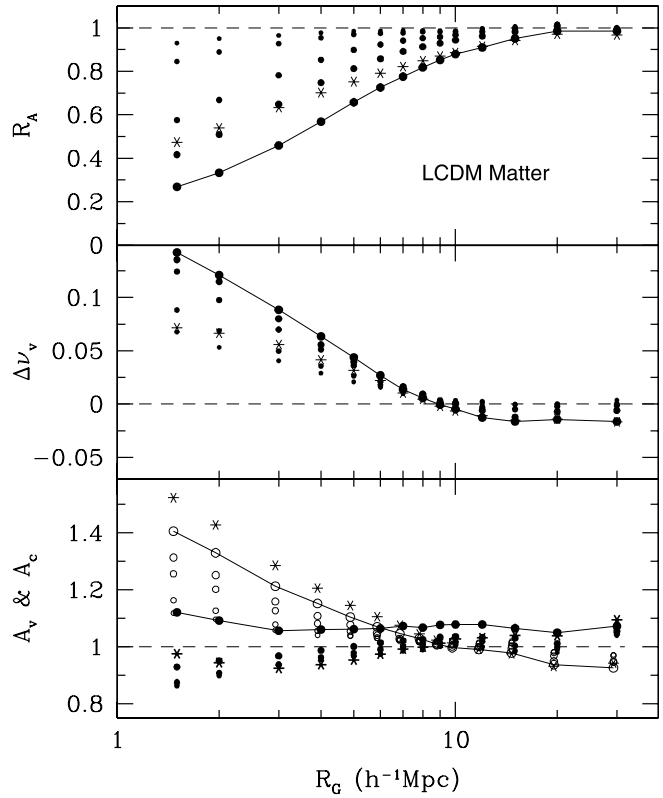

FIG. 1.—Genus-related statistics for dark matter measured from the LCDM 1024 simulation. Filled circles with different sizes represent the statistics at redshifts $z = 0$, 1, 2, 5, and 8. The largest filled circles connected by lines are for $z = 0$, and the smallest are for $z = 8$. In the bottom panel, filled circles are A_C, and open circles are A_V, which are slightly shifted to avoid confusion. Asterisks are the statistics measured in redshift space. In the bottom panel, heavy asterisks are A_C, and light asterisks are A_V.

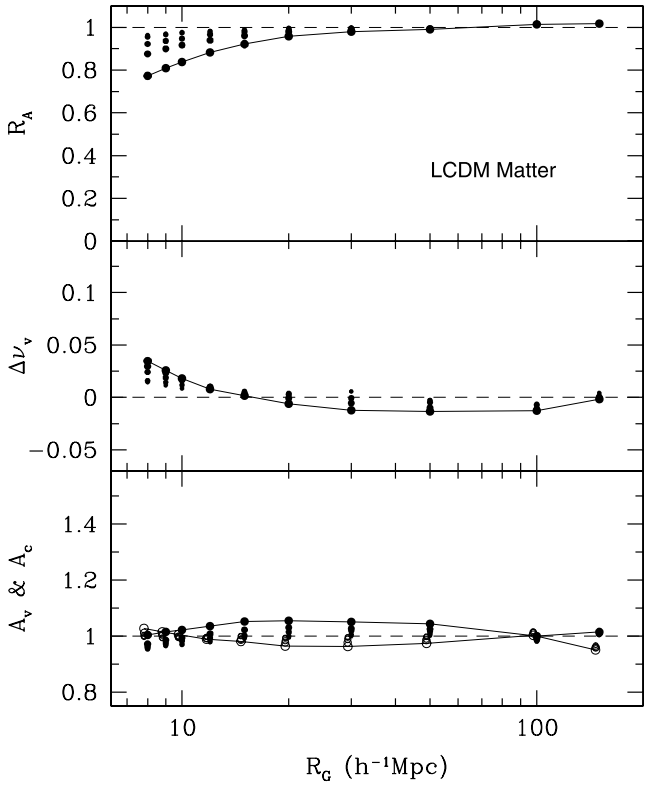

FIG. 2.—Same as Fig. 1, but for statistics calculated from the LCDM 5632 simulation. Note that the data at $z = 8$ and 5 are almost overlapping. Only measurements in real space are plotted.

calculated at seven epochs with redshifts z from 0 to 8, but we show results only at $z = 0$, 1, 2, 5, and 8 to avoid overcrowding of points in the figures.

5.1. ΛCDM Dark Matter

The mean particle separation of the LCDM 1024 simulation is 0.5 h^{-1} Mpc, and we explore the topology of the dark matter distribution from $R_G = 1.5$ to 30 h^{-1} Mpc. The size of the density array is 2048^3, so the smoothing length is at least 3 times larger than the pixel size (thus avoiding discreteness effects). The results for the genus-related statistics are shown in Figure 1 as filled and open circles. Filled circles with different sizes represent the statistics at different redshifts from $z = 0$ (*largest circles connected by solid lines*), 1, 2, 5 to 8 (*smallest circles*). The dark matter in the ΛCDM universe clearly shows an intriguing development of small-scale topology in the cases of $\Delta\nu$ and A_V statistics in a direction opposite that at large scales. The shift parameter $\Delta\nu$ rapidly goes to positive values at $R_G < 9\ h^{-1}$ Mpc. But at scales $R_G > 9\ h^{-1}$ Mpc, it slowly moves in the negative direction and continues to be negative even at the 30 h^{-1} Mpc scale. All these genus curves have a spongelike topology ($G > 0$) at the median density contour, so we would not call the negative and positive shifts of the central part of the genus curve as in the direction of "meatball" and "bubble" topologies, respectively, since their correspondence does not seem to be so simple. The transition scale of $\Delta\nu$ from positive to negative shift agrees with the analytic prediction of § 5.6.

In Figure 2 the genus-related statistics calculated from the LCDM 5632 simulation are plotted to show their behavior at larger scales. Note that the power spectrum of LCDM 5632 is slightly different from that of LCDM 1024, thus making the transition scale of $\Delta\nu$ occur at different R_G. It can be seen that non-Gaussianity is visible up to the scale $\sim$100 h^{-1} Mpc. But using the analytic estimation of the non-Gaussianity effects of gravitational evolution in this weakly nonlinear scale given in § 5.6, one could draw conclusions on the Gaussianity of the initial density field from data with smoothing lengths much smaller than 100 h^{-1} Mpc if the matter distribution can be used.

The parameter A_V for voids (Figs. 1 and 2, *bottom, open circles*) shows a behavior similar to that of the shift parameter. At scales below 10 h^{-1} Mpc, voids are broken into many pieces and the number of voids exceeds the Gaussian value predicted by the middle part of the genus curve (see Fig. 1). But at larger scales voids percolate, and the number of voids is slightly lower than the Gaussian value (see Fig. 2). On the other hand, the parameter A_C for clusters (Figs. 1 and 2, *bottom, filled circles*) behaves differently. It tends to increases at all scales at the present epoch. The speed with which new high-density clumps stick up above the threshold and appear in the sample is faster than that of merging and disappearance of existing clumps. But at very small scales ($R_G \leq 2\ h^{-1}$ Mpc) the merging speed wins over the sticking-up speed at high redshifts ($z \geq 5$), and subsequently the situation reverses. At large scales, the sticking-up of clusters and merging of voids are the dominant processes (Fig. 2). It should be noted that gravitational evolution only makes both parameters A_V and A_C increase over 1 at scales below 10 h^{-1} Mpc at the present epoch. Therefore, the observed value of the void abundance parameter A_V, which is less than 1 (Park et al. 2005), must be due to strong biasing effects, which tend to make small voids merge with one another. This can be achieved if galaxies do not form in weak walls and filaments of large-scale structure dividing small voids.

The amplitude drop parameter shown in the top panel of Figure 1 evolves very rapidly at scales below about 10 h^{-1} Mpc as the gravitational evolution proceeds. Its scale dependence is again determined by the characteristic shape of the power spectrum of the ΛCDM model.

Also shown in the figures are the genus-related statistics measured in redshift space at $z = 0$ (*asterisks*). We adopt the far-field approximation to the redshift distortion of the density field. Displacement of particles is thus assumed to occur only along the direction of a coordinate axis. We average three genus curves measured from redshift space density fields, each of which is perturbed in the direction of each coordinate axis using the periodic boundary condition. Genus and the power spectrum of the density field in redshift space are measured to calculate the genus-related statistics. The amplitude drop parameter R_A increases in redshift space because the amplitude of the random-phase genus curve ($A_{\rm PS}$ in eq. [7]) drops more than that of nonlinear genus curve ($A_{\rm obs}$) due to the randomization effects of small-scale peculiar velocity. Effects of redshift space distortions on the genus curve have been previously studied by Melott et al. (1988). They have reported that the effects are negligible when a smoothing larger than the correlation length is applied to the density field; the linear regime calculation of Matsubara (1996) has supported their claim. Subsequently, redshift space distortion effects have been generally ignored in the genus analyses. This is qualitatively true for the matter field of the ΛCDM model, where the correlation length is about 5.5 h^{-1} Mpc at $z = 0$ and smoothing lengths larger than this are studied. However, as can be seen in our figures, there are nonnegligible systematic effects of redshift space distortion on the genus-related statistics at the small smoothing scales we are interested in. An example is the A_C parameter (Fig. 1, *bottom, heavy asterisks*). Being a measure of the topology of high-density regions, A_C is most sensitive to the peculiar velocity field.

5.2. ΛCDM Biased Peak Particles

We use the peaks in the initial Gaussian density field as the biased galaxy particles. They are defined by the threshold level $\nu_{\rm th}$ and the galaxy scale R_s (Park & Gott 1991), which are chosen so that the resulting biased particles approximate the distribution of galaxies at the present epoch. When we require them to have $\sigma_{\rm pk,8} = 1$ and to have a correlation function (CF) close to the observed galaxy CF at $z = 0$, we find a set, $\nu_{\rm th} = 0.05$ and $R_s = 0.763\,h^{-1}$ Mpc in our ΛCDM universe with $\sigma_{m,8} = 0.9$. The number density of the peaks is much lower than that of CDM particles, and the genus is measured only at scales $R_G \geq 5\ h^{-1}$ Mpc. The simulation used for identifying the biased peak particles is the ΛCDM model evolved by the PM code in a 2048^3 mesh spanning 409.6 h^{-1} Mpc along a side. Its small pixel size (0.2 h^{-1} Mpc) allows us to look for density peaks at the galaxy scale R_s. The genus-related statistics of the biased peak particles are shown in Figure 3. Although our biased density peaks collapse at a specific epoch and can be considered as galaxies after then, we plot the statistics of the biased particles at all epochs after $z = 8$ for theoretical interest.

They behave essentially in the same way as those for CDM, but there are some changes. Similarly to the case of CDM, the peak particles develop a negative shift $\Delta\nu$ at scales larger than 6 h^{-1} Mpc and a positive shift at smaller scales. And the cluster abundance parameter A_C increases at all scales above 5 h^{-1} Mpc. However, the void abundance parameter A_V (Fig. 3, *open circles*) shows more changes. Namely, at scales smaller than about 7 h^{-1} Mpc, the biasing prescription makes small voids percolate,

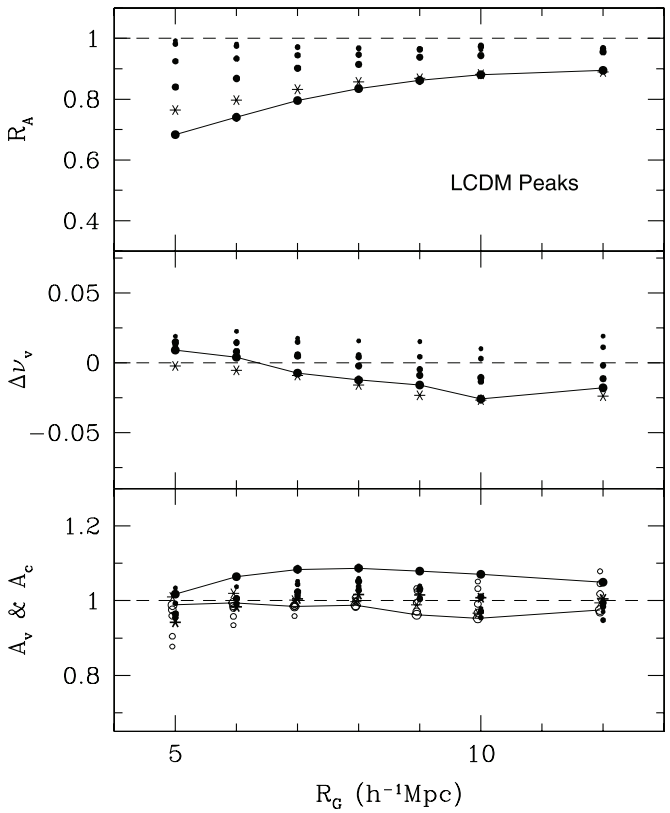

FIG. 3.—Genus-related statistics for the biased peaks calculated from the ΛCDM 410 simulation. Notations are the same as in Fig. 1.

and A_V become less than 1 at high redshifts. As noted above, gravitational evolution only makes A_V increase above 1 at scales less than 10 h^{-1} Mpc, contrary to observations. Here we have a specific example of a galaxy formation mechanism that allows existing voids to percolate strongly enough to overcome the nonlinear gravitational effect of opening of new voids and makes A_V less than 1.

The asterisks in Figure 3 are the statistics measured in redshift space at $z = 0$. The effect significantly decreases A_C (Fig. 3, *bottom, heavy asterisks*) at all scales explored, as dense clusters are spread along fingers of God. It can be noted that the void abundance parameter is not much affected by the redshift space distortion because empty regions are much more stable to the distortion compared to dense clumps. This observation is also true for other tracers used in this work. Given its insensitivity to redshift space distortion, A_V is a crucial statistic telling the story of galaxy formation in a less distorted way.

5.3. ΛCDM Dark Halos

The biased particles studied above are the density peaks in the Gaussian initial density field. This structure formation scheme assumes that galaxies form at the maxima in the primordial density fluctuations. It can be shown that these actually correspond well to collapsed dark halos at the final epoch of simulations (Park & Gott 1991). However, it would be good to check the idea and to recompute the same statistics using physically bound dark halos identified in high-resolution simulations. Another important difference between the biased peak particles and dark halos is that the formation of tracers is naturally incorporated in the genus analysis in the case of dark halos. Since we need high resolution for halo formation and identification and

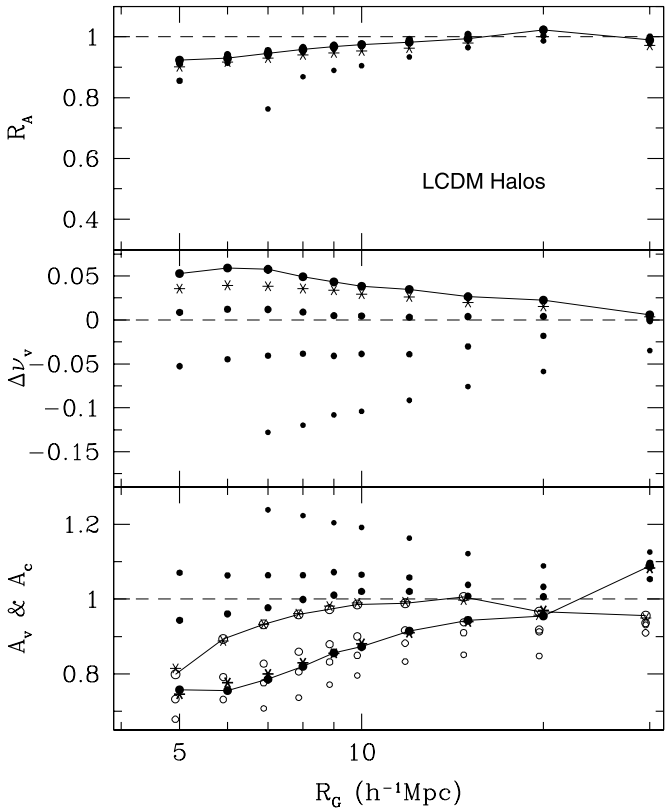

FIG. 4.—Genus-related statistics for the dark halos calculated from the LCDM 1024 simulation. Notations are the same as in Fig. 1. Since the number density of dark halos at $z = 8$ and 5 is too low, we show the results at $z = 0$, 1, 2, and 3.5. At $z = 3.5$ (*smallest points*) the genus is measured at $R_G \geq 7\ h^{-1}$ Mpc.

large volume for high statistical significance, the LCDM 1024 simulation is used. The minimum halo mass identified is $5 \times 10^{11}\ M_\odot$ (53 particles). With the dark halo samples obtained from this simulation, topology of the dark halo distribution is studied at scales from 5 to 30 h^{-1} Mpc at $z = 0$. At higher redshifts, the minimum smoothing length used becomes larger as the dark halos collapsed by then become rarer.

The genus-related statistics measured for the dark halos in the ΛCDM model are shown in Figure 4. Topology of ΛCDM dark halos is very different from those of underlying dark matter or biased peak particles. The shift parameter $\Delta\nu$ starts from large negative values at high redshifts when only the densest regions can collapse. Consistent with this behavior, the A_C parameter is greater than 1, and A_V is less than 1 at high redshifts. At lower redshifts, the topology of the dark halo distribution evolves strongly. Here $\Delta\nu$ becomes positive and A_C becomes less than 1. This is opposite what we have seen in the case of CDM and biased peak particle distributions. The A_V parameter still stays below 1 but has increased from its high-redshift value, which is consistent with the case of biased peak particles. The A_C of dark halos rapidly decreases at low redshift, while that of peak particles keeps increasing. This is because the dark subhalos merge to form one huge halo at centers of clusters of halos, thus decreasing the number of subhalos or reducing the richness of clusters as nonlinear evolution proceeds at small scales. This merging process within clusters does not exist for peak particles because peak particles never lose their identity and the clusters of peak particles get richer as they become more compact. The reality might be somewhere between these two extremes. Comparison of Figure 4 with Figures 1–3 demonstrates sensitivity of the topology to the galaxy formation mechanism. Since galaxies show different topology depending on their internal physical properties, topology analysis can be used to discriminate among different galaxy formation mechanisms for different species of galaxies.

Hikage et al. (2003) have calculated the biasing and genus of dark matter halos as a function of halo mass and smoothing scale using the Hubble volume simulation. They have found that the halo biasing effects on the genus are comparable to the non-Gaussianity due to the nonlinear gravitational evolution. This is consistent with our results that changes of the genus-related statistics due to gravitational evolution at the $R_G = 30\ h^{-1}$ Mpc scale is of the order of that due to tracer difference. Hikage et al. (2003) have studied topology of halo distribution at $R_G \geq 30\ h^{-1}$ Mpc. However, at $R_G = 30\ h^{-1}$ Mpc their results are thought to be affected by discreteness effects because the mean separation of their halo subsets is only about 44 h^{-1} Mpc. In topology analysis of a set of points, the smoothing length should be larger than the mean tracer separation to avoid systematic discreteness effects, or some correction should be made to remove the effects (Park et al. 2005). The large pixel size of 23 h^{-1} Mpc used in their analysis may have also caused some discreteness effects at that smoothing scale. In general, one wants the smoothing length R_G to be at least 1.77 times the pixel size to avoid discreteness effects (e.g., Hamilton et al. 1986). To identify halos, they have used the friends-of-friends algorithm, which is known to miss subhalos within large halos and often produces unphysical halos connected by narrow chains of particles. Therefore, it is not easy to directly compare their results with those of the current work in detail. But our results qualitatively agree with their conclusion that non-Gaussianity induced by halo biasing is comparable to that by the nonlinear gravitational evolution.

5.4. *Halo Occupation Distribution (HOD) Galaxies*

A halo identified in the *N*-body simulation might not contain a galaxy or could host more than one galaxy. Therefore, although dark halos might be a better tracer of the observed galaxies than matter, they might not be representing galaxy distribution well enough to allow quantitative comparisons. We address this problem by introducing the HOD prescription to locate "galaxies" within our dark halos. We adopt the following recipe of Zehavi et al. (2005). A central galaxy is assigned to a halo if its mass M exceeds $M_{\rm min}$, and the central galaxy can have satellites. The mean number of satellite galaxies is given by a power law $\langle N_{\rm sat}\rangle = (M/M_1)^\alpha$, and they have a Poisson distribution. The satellites are randomly located at distances of 0.3 h^{-1} Mpc from the central galaxy. This does not change our results because the minimum smoothing scale adopted for analysis of the HOD galaxies is 5 h^{-1} Mpc. We use, as a toy model, the HOD parameters $\log M_{\rm min} = 11.76$, $\log M_1 = 13.15$, and $\alpha = 1.13$ given by Table 3 of Zehavi et al., corresponding to galaxies with an absolute r magnitude cut of $M_r = -19.5$ in the SDSS.

In Figure 5 we show the genus-related statistics calculated from distribution of galaxies assigned within dark halos of the LCDM 1024 simulation according to the HOD prescription. The correlation length of these model galaxies is $5.6\ h^{-1}$ Mpc, similar to that of bright optical galaxies. Only the results at $z = 0$ are shown. Comparing the statistics with those of dark halos at $z = 0$, we find $\Delta\nu$ becomes less positive, A_C is increased, and A_V is decreased. These change the topology of our HOD galaxies, making it more compatible with that observed for SDSS galaxies (Park et al. 2005). Topology depends on the type of observed galaxies, but one phenomenon consistently found in observations is that the A_V parameter is less than 1. This behavior is seen

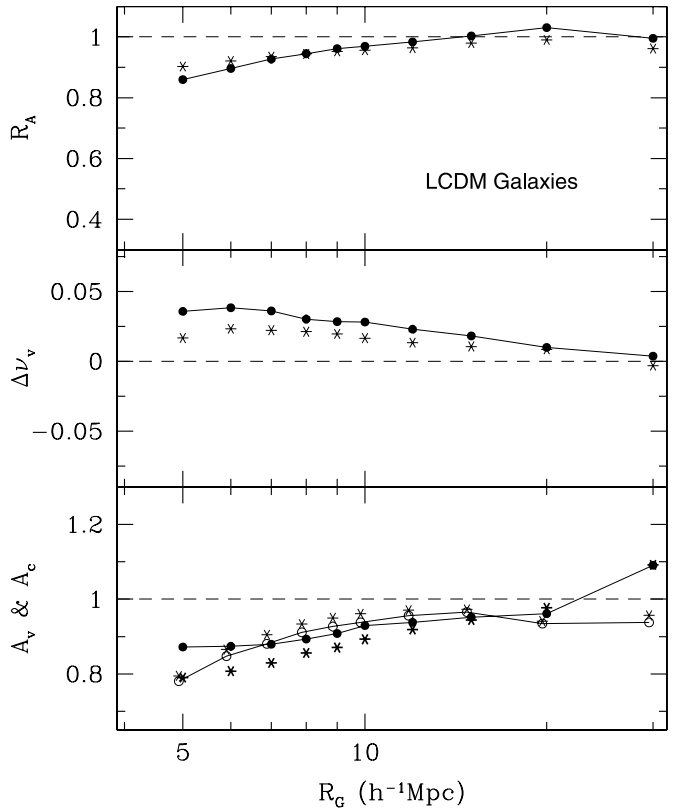

FIG. 5.—Genus-related statistics for the "galaxies" derived from the dark halos of the LCDM 1024 simulation. Notations are the same as in Fig. 1. Only the results at $z = 0$ are shown.

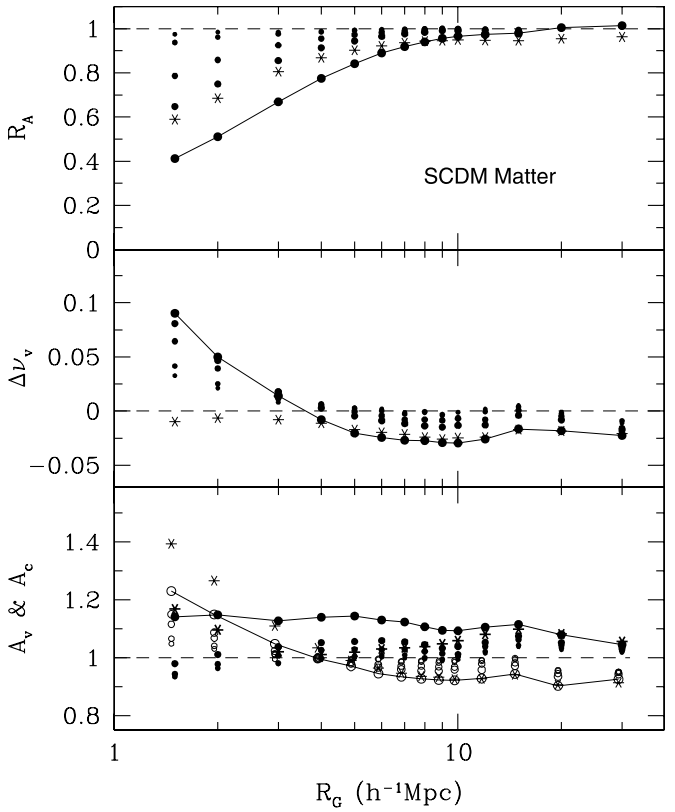

FIG. 6.—Genus-related statistics for dark matter measured from the SCDM 1024 simulation. Notations are the same as in Fig. 1.

in the distribution of our HOD galaxies. However, the observed A_C parameter is typically greater than A_V, which does not quite agree with the HOD galaxies. The HOD method seems to be promising in explaining not only the one-point and two-point functions of galaxy distribution but also functions of high-order moments like genus. However, more detailed comparisons have to be made to confirm it.

Benson et al. (2001) have used a semianalytic model of galaxy formation to obtain the distribution of model galaxies and to measure the genus curves at smoothing lengths of 4.24 and 5.66 h^{-1} Mpc at redshifts $z = 0$ and 1. But they have not been able to detect the difference between the genus curves for the dark matter and the model galaxies due to sparseness and smallness of their simulation data.

5.5. *SCDM Case*

As a fiducial model we consider the SCDM model to study the dependence of topology on cosmology. In this model $\Omega_m = 1$ and $h = 0.5$, and we adopt a bias factor $b = 1.5$ and the fitting formula of Bardeen et al. (1986) for the power spectrum. Figure 6 shows that the matter distribution of the SCDM universe has qualitatively the same topology as that of the ΛCDM universe, except that the characteristic scales are moved down in the cases of $\Delta\nu$ and A_V. The switching from negative to positive shift occurs at ~ 4 h^{-1} Mpc, and the switching from sub-Gaussian to super-Gaussian amplitude for the void part of the genus curve occurs at a similar scale. This change in the characteristic scales is the direct consequence of the change in the shape of power spectrum. Figure 7 shows the statistics for the biased peak particles found in the SCDM simulation. For $\Delta\nu$ a negative shift prevails at all scales, and the redshift space distortion effects make little change

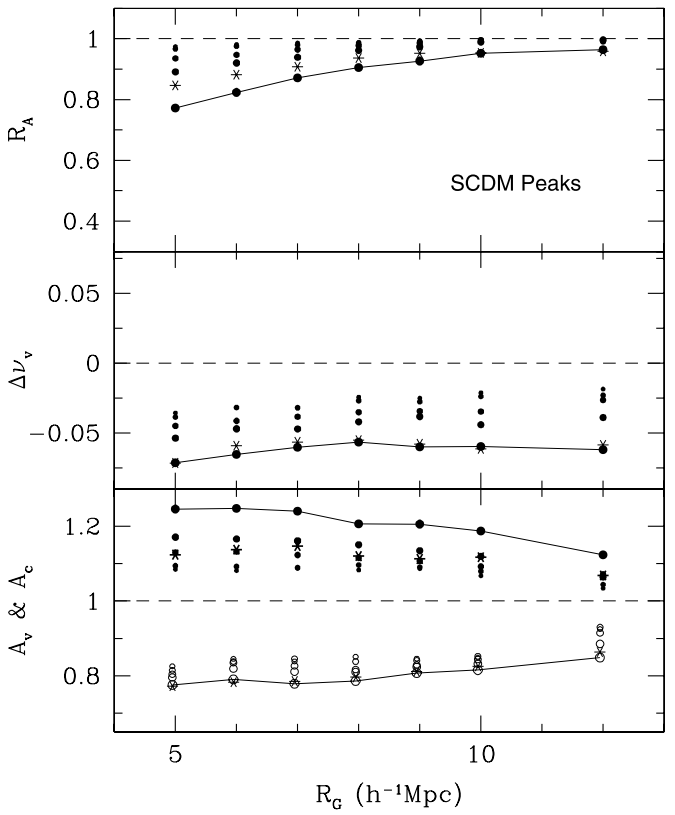

FIG. 7.—Genus-related statistics for the biased peaks measured from the SCDM 410 simulation. Notations are the same as in Fig. 1.

in $\Delta\nu$. Gravitational evolution makes the A_C parameter increase above 1, as in the ΛCDM case, while the redshift space distortion effects make it decrease. The void abundance parameter A_V is significantly less than 1 due to the biasing effects at small scales and is hardly affected by the redshift space distortion, as in the ΛCDM case.

5.6. *Comparison with Perturbation Theory*

Matsubara (1994) has obtained a formula for the genus curve modified due to gravitational evolution in the weakly nonlinear regime by perturbatively expanding the statistic in $\sigma_0 = (\delta\rho/\rho)_{\rm rms}$, the rms fluctuation of an overdensity field smoothed over a given scale. The nonlinear correction in the genus curve to the first order in σ_0 is an odd function of ν and, therefore, causes a shift and an asymmetry between the high- and low-density regions. It is hoped that the gravitational evolution effects on genus in the weakly nonlinear regime can be modeled by this analytic theory. When the volume threshold level is used, the three-dimensional genus expanded to the first order in σ_0 is given by (Matsubara 2003)

$$G(\nu_f) = \frac{1}{(2\pi)^2}\left(\frac{\sigma_1}{\sqrt{3}\sigma_0}\right)^3 e^{-\nu_f^2/2} \times\left\{1-\nu_f^2-\left[\left(S^{(1)}-S^{(0)}\right)\left(\nu_f^3-3\nu_f\right)+\left(S^{(2)}-S^{(0)}\right)\nu_f\right]\sigma_0\right\}, \tag{9}$$

where the variance parameters are

$$\sigma_j^2(R) = \int \frac{k^2\,dk}{2\pi^2}\,k^{2j}P(k)W^2(kR), \tag{10}$$

the window function is a Gaussian $W(kR) = \exp(-k^2R^2/2)$, and $S^{(i)}$ are the skewness parameters, defined as

$$S^{(0)} = \frac{\langle\delta^3\rangle}{\sigma_0^4} = \frac{1}{\sigma_0^4}\int\frac{d^3k_1}{(2\pi)^3}\frac{d^3k_2}{(2\pi)^3}\,B(k_1,k_2,k_{12}), \tag{11}$$

$$S^{(1)} = -\frac{3}{4}\frac{\langle\delta^2\nabla^2\delta\rangle}{\sigma_0^2\sigma_1^2} = \frac{3}{4\sigma_0^2\sigma_1^2}\int\frac{d^3k_1}{(2\pi)^3}\frac{d^3k_2}{(2\pi)^3}\,k_{12}^2B(k_1,k_2,k_{12}), \tag{12}$$

$$S^{(2)} = -\frac{9}{4}\frac{\langle(\nabla\delta\cdot\nabla\delta)\nabla^2\delta\rangle}{\sigma_1^4} = \frac{9}{4\sigma_1^4}\int\frac{d^3k_1}{(2\pi)^3}\frac{d^3k_2}{(2\pi)^3}\,\boldsymbol{k}_1\cdot\boldsymbol{k}_2k_{12}^2B(k_1,k_2,k_{12}), \tag{13}$$

where $k_{12} = |\boldsymbol{k}_1+\boldsymbol{k}_2|$ and B is the bispectrum. The skewness parameters can be calculated from (Matsubara 2003)

$$S^{(0)} = (2+E)S_0^{11} - 3S_1^{02} + (1-E)S_2^{11}, \tag{14}$$

$$S^{(1)} = \frac{3}{2}\left[\frac{5+2E}{3}S_0^{13} - \frac{9+E}{5}S_1^{22} - S_1^{04} + \frac{2(2-E)}{3}S_2^{13} - \frac{1-E}{5}S_3^{22}\right], \tag{15}$$

$$S^{(2)} = 9\left[\frac{3+2E}{15}S_0^{33} - \frac{1}{5}S_1^{24} - \frac{3+4E}{21}S_2^{33} + \frac{1}{5}S_3^{24} - \frac{2(1-E)}{35}S_4^{33}\right], \tag{16}$$

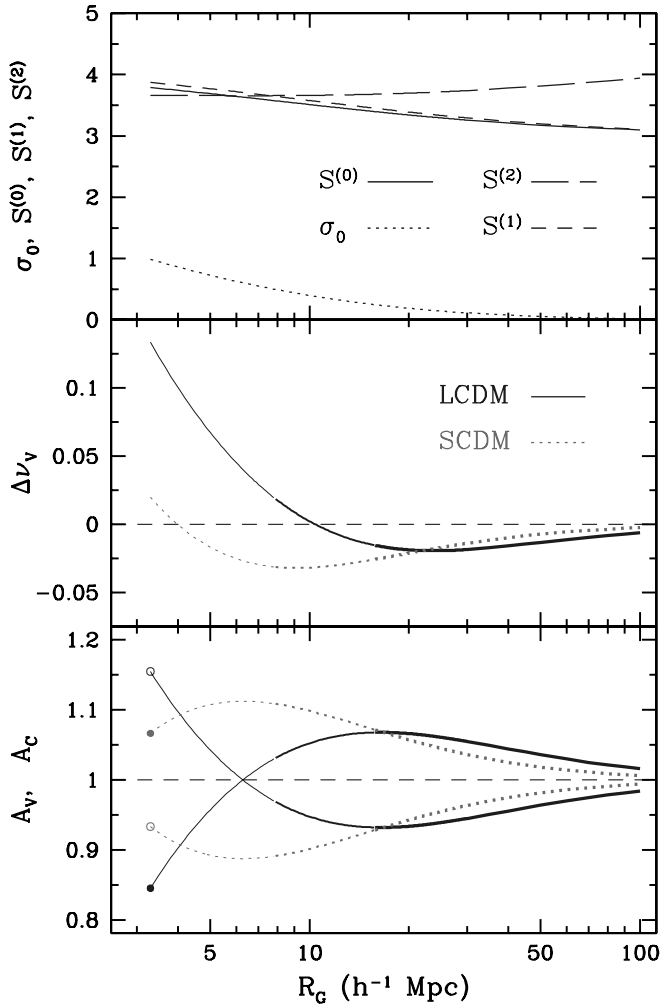

FIG. 8.—Genus-related statistics at $z = 0$ according to Matsubara's perturbation theory. In the middle and bottom panels, thick curves are for scales with $\sigma_0 < 0.25$, medium-thickness curves for $0.25 \le \sigma_0 < 0.5$, and thin curves for $0.5 \le \sigma_0 < 1.0$. In the top panel, the rms deviation of the density fluctuation and skewness parameters are plotted.

where

$$E \approx \frac{3}{7}\Omega_m^{-1/30} - \frac{\Omega_\Lambda}{80}\left(1-\frac{3}{2}\Omega_\Lambda\log_{10}\Omega_m\right), \tag{17}$$

and

$$S_m^{\alpha\beta} = \frac{\sqrt{2\pi}}{\sigma_0^4}\left(\frac{\sigma_0}{\sigma_1 R}\right)^{\alpha+\beta-2} \times\int\frac{l_1^2\,dl_1}{2\pi^2R^3}\frac{l_2^2\,dl_2}{2\pi^2R^3}P\left(\frac{l_1}{R}\right)P\left(\frac{l_2}{R}\right)e^{-l_1^2-l_2^2}l_1^{\alpha-3/2}l_2^{\beta-3/2}I_{m+1/2}(l_1l_2). \tag{18}$$

Here P is the linear power spectrum and I_ν are the modified Bessel functions.

We have performed the above integrals to get the skewness parameters for our ΛCDM and SCDM models as a function of smoothing length R_G. The curves in Figure 8 show the genus-related statistics predicted by equation (9) for the ΛCDM and SCDM models at the present epoch $z = 0$. In the top panel the rms density fluctuation σ_0 and the skewness parameters are shown. The differences between the skewness parameters in equation (9)

are very small, as can be seen here, and make the genus as a function of ν_f rather insensitive to gravitational evolution. According to perturbation theory, the amplitude of the genus curve remains the same in the weakly nonlinear regime. This is certainly not true because the density field starts to build phase correlations and the genus amplitude starts to decrease as soon as the gravitational evolution occurs. The behaviors of the $\Delta\nu$, A_C, and A_V parameters predicted by equation (9) are remarkably similar to those seen in Figures 1 and 6. This is an important confirmation of Matsubara's theory. The one major failure of the analytic prediction is for the A_C parameter at small nonlinear scales. At high redshifts, A_C decreases below 1 as high-density clumps merge together, as predicted by analytic theory. But at lower redshifts, A_C increases to become greater than 1 as the merging rate slows down and the rate at which new clumps appear becomes higher.

Matsubara (1996) has derived the genus in redshift space in the linear regime. The genus in redshift space predicted by linear theory is

$$G^{(s)}(\nu) = \frac{3\sqrt{3}}{2}\sqrt{C}(1-C)G^{(r)}(\nu), \tag{19}$$

where $G^{(r)}(\nu)$ is the genus curve in real space,

$$C = \frac{1}{3}\left[\frac{1+(6/5)(f/b)+(3/7)(f/b)^2}{1+(2/3)(f/b)+(1/5)(f/b)^2}\right], \tag{20}$$

b is the bias factor, and

$$f = \frac{d\ln D}{d\ln a} \approx \Omega_m^{0.6} + \frac{\Omega_\Lambda}{70}\left(1+\frac{\Omega_m}{2}\right), \tag{21}$$

where D is the linear growth factor and a is the expansion parameter. The formula says that the redshift space distortion does not alter the shape of the genus curve and only affects its amplitude. For matter in our ΛCDM model, $b = 0.9, f = 0.468$, and $C = 0.414$, and the amplitude drops by a factor of 0.980; while in the SCDM model, which has $b = 1.5, f = 1$, and $C = 0.433$, the factor is 0.970. In the linear regime, the genus amplitude calculated from the redshift space power spectrum is equal to that from the real space power spectrum, since the shape of the power spectrum remains the same. This makes the denominator of the amplitude drop parameter R_A unchanged in redshift space and makes R_A itself decrease by the above factors in the ΛCDM and SCDM models. This can be observed in Figures 1 and 6 at scales $R_G \geq 20\ h^{-1}$Mpc.

Matsubara & Suto (1996) have used N-body simulations to examine the redshift space distortion effects on genus. They have reported that the amplitude of the genus curve is suppressed more than that expected by linear theory but that its shape in redshift space still remains the same down to weakly nonlinear scales. We have also shown that the redshift space distortion effects on the genus curve are small in the linear and quasi-linear scales. But it should be pointed out that the high-threshold part of the genus curve (namely, the A_C parameter) is more affected.

Comparisons of numerically calculated genus with theoretical predictions are useful. But so far theories have mainly concerned themselves with the development of non-Gaussianity in the local density field rather than changes in topology. Our genus metastatistics are directly addressing questions about the gravitational evolution of topology and the effects of biasing and redshift space distortion on topology.

6. CONCLUSIONS

We have studied dependence of the genus statistic on cosmology, tracer, redshift, and Gaussian smoothing scale. We summarize our findings.

1. The shift parameter $\Delta\nu$ of the genus curve shows a strong scale dependence whose characteristics are determined by the shape of the initial power spectrum. For the matter distribution in the ΛCDM model, the negative-to-positive transition occurs at $\sim 9\ h^{-1}$ Mpc, while it is at about $4\ h^{-1}$ Mpc for SCDM. Below these scales, gravitational evolution causes strong positive shifts starting from high redshifts. At larger scales, the gravitational evolution produces weak negative shifts. This trend enhances as the evolution proceeds. When the topology tracers are biased peak particles instead of CDM particles, evolution of the genus curve is qualitatively similar. But the positive-to-negative transition scale is different, and at small scales $\Delta\nu$ keeps slowly decreasing, which is opposite the case of CDM particles. We have demonstrated that galaxies can have a topology very different from that of matter on small scales. The $\Delta\nu$ parameter measured from the dark halo and HOD "galaxy" distributions is positive at scales between 5 and $30\ h^{-1}$ Mpc and becomes more positive due to the combined effects of formation of new objects and gravitational clustering. This trend is opposite that seen in distributions of matter and biased peak particles at scales larger than $9\ h^{-1}$ Mpc. It remains to be seen which value of the shift parameter the distribution of real galaxies has. The redshift space distortion systematically decreases $\Delta\nu$ in the ΛCDM universe, and the effects are significant at scales $\leq 5\ h^{-1}$ Mpc. We can in principle correct for these redshift space distortion effects on $\Delta\nu$ by using the observationally measured line-of-sight velocity dispersion to correct the shift parameter at both large and small scales for the study of primordial density field and galaxy formation mechanisms.

2. The amplitude drop parameter is more difficult to measure than the genus curve alone because it requires an additional accurate measurement of the power spectrum for each tracer of topology. Direct consequence of genus amplitude drop is the phase correlation of the density field, and the phase correlation depends on the shape of the initial density power spectrum and the biasing. We have found that the dark halos and the HOD galaxies show a very small genus amplitude drop with $0.9 \leq R_A \leq 1$ down to the scale $5\ h^{-1}$ Mpc with little scale dependence and that it hardly changes due to gravitational evolution or peculiar motions. This might be incompatible with the observationally measured value of about 0.6 at $5\ h^{-1}$ Mpc for the *IRAS* Point Source Catalogue Redshift Survey (Canavezes et al. 1998) or for the Center for Astrophysics Survey (Vogeley et al. 1994). Satisfying the constraint from the genus amplitude drop can be a challenge for HOD modeling of galaxy formation.

3. The void abundance parameter A_V of the dark matter distribution strongly increases above the Gaussian value below $10\ h^{-1}$ Mpc but gently drops below 1 at larger scales as the gravitational evolution proceeds. This is true for both ΛCDM and SCDM models, although their transition scales are different. While gravitational evolution always raises A_V at small scales, biasing can lower it below 1, as can be seen for the biased peak particles, dark halos, and HOD galaxies. Even the direction of evolution of A_V (and A_C) can be changed by biasing. Since A_V is observed to be less than 1 for the SDSS galaxies (Park et al. 2005), this fact is strong evidence for the existence of biasing in the distribution of galaxies with respect to matter. Fortunately, A_V at small scales is hardly affected by the redshift distortion effects and can give faithful constraints on galaxy formation in underdense regions.

We have considered only three mechanisms for galaxy formation. The peak biasing scheme is able to explain the stronger clustering amplitude for rarer objects (Kaiser 1984). But we have considered only one version of the peak biasing scheme, where the threshold for galaxies is a step function, and have not taken into account merging (cf. Narayanan et al. 2000 for various biasing models). The first assumption affects the voids, and the second affects the clusters. The arbitrariness of the threshold function can be removed by using the dark halos that have collapsed and are self-bound physical objects. But the dark halos also cannot fully trace galaxies because the mass function of dark halos continuously extends up to supercluster scales and does not show a natural cutoff for galaxies. Some of them with small masses may have lost baryons in high-density environments and have not been able to form stars. The HOD galaxies seem to approximate the distribution of real galaxies better than the dark halos because the A_V parameter is closer to observations for the HOD galaxies, although the cluster abundance parameter A_C may be still too small (cf. Park et al. 2005).

While galaxy formation and evolution in a high-density environment are complicated due to the merging of structures and the high ram pressure of the intergalactic medium (Gunn & Gott 1972), it may be relatively easier to model galaxy formation in low-density regions. For example, biased peak particles, dark halos, and HOD galaxies all produce A_V smaller than 1, consistent with observations. But their A_C are wildly different. Therefore, although identification of the biased peaks and dark halos with galaxies is not a good approximation in high-density regions, they seem to trace galaxies better in underdense regions for which there is a sensitive measure like the void abundance parameter A_V. It should be emphasized that the cosmic voids have not been studied as extensively as clusters and superclusters, and it is only in recent years that voids have begun to be actively studied (Hoyle & Vogeley 2004; Sheth & van de Weygaert 2004; Rojas et al. 2005; Colberg et al. 2005). After all, voids are not the places where there is nothing, but places where history of the universe is better kept. With the advent of new large observational data sets like the SDSS sample, we can hope to better to understand the formation mechanism of each species of galaxy through the topology analysis. We are currently studying the topology of galaxies divided into subgroups with different internal physical properties.

C. B. P. is supported by the Korea Science and Engineering Foundation (KOSEF) through the Astrophysical Research Center for the Structure and Evolution of the Cosmos (ARCSEC) and through grant R01-2004-000-10520-0. C. B. P. and J. H. K. also acknowledge the support of Korea Institute of Science and Technology Information through the Grand Challenge Support Program. J. R. G. is supported by NSF grant AST 04-06713.

REFERENCES

Bareen, J. M., Bond, J. R., Kaiser, N., & Szalay, A. S. 1986, ApJ, 304, 15
Benson, A. J., Frenk, C. S., Baugh, C. M., Cole, S., & Lacey, C. G. 2001, MNRAS, 327, 1041
Canavezes, A, et al. 1998, MNRAS, 297, 777
Colberg, J. M., Sheth, R. K., Diaferio, A., Gao, L., & Yoshida, N. 2005, MNRAS, 360, 216
Dubinski, J., Kim, J., Park, C., & Humble, R. 2004, NewA, 9, 111
Eisenstein, D. J., & Hu, W. 1998, ApJ, 496, 605
Gott, J. R., Melott, A. L., & Dickinson, M. 1986, ApJ, 306, 341
Gott, J. R., et al. 1989, ApJ, 340, 625
Gunn, J. E., & Gott, J. R. 1972, ApJ, 176, 1
Hamilton, A. J. S., Gott, J. R., & Weinberg, D. H. 1986, ApJ, 309, 1
Hikage, C., Taruya, A., & Suto, Y. 2003, PASJ, 55, 335
Hoyle, F., & Vogeley, M. S. 2004, ApJ, 607, 751
Kaiser, N. 1984, ApJ, 284, L9
Kim, J., & Park, C. 2004, preprint (astro-ph/0401386)
Matsubara, T. 1994, ApJ, 434, L43
———. 1996, ApJ, 457, 13
Matsubara, T. 2003, ApJ, 584, 1
Matsubara, T., & Suto, Y. 1996, ApJ, 460, 51
Mecke, K. R., Buchert, T., & Wagner, H. 1994, A&A, 288, 697
Melott, A. L., Weinberg, D. H., & Gott, J. R. 1988, ApJ, 328, 50
Narayanan, V. K., Berlind, A. A., & Weinberg, D. H. 2000, ApJ, 528, 1
Park, C. 1990, MNRAS, 242, 59P
———. 1997, J. Korean Astron. Soc., 30, 191
Park, C., & Gott, J. R. 1991, ApJ, 378, 457
Park, C., Gott, J. R., & da Costa, L. N. 1992, ApJ, 392, L51
Park, C., et al. 2005, ApJ, 633, 11
Rojas, R. R., Vogeley, M. S., Hoyle, F., & Brinkmann, J. 2005, ApJ, 624, 571
Schmalzing, J., & Buchert, T. 1997, ApJ, 482, L1
Sheth, R. K., & van de Weygaert, R. 2004, MNRAS, 350, 517
Springel, V., et al. 1998, MNRAS, 298, 1169
Vogeley, M. S., Park, C., Geller, M. J., Huchra, J. P., & Gott, J. R. 1994, ApJ, 420, 525
Zehavi, I., et al. 2005, ApJ, 630, 1